Applied Catalysis B: Environmental 170-171 (2015) 34–42

Contents lists available at ScienceDirect

Applied Catalysis B: Environmental

journal homepage: www.elsevier.com/locate/apcatb

CoZSM-11 catalysts for N_2O decomposition: Effect of preparation methods and nature of active sites

Pengfei Xie[a], Yajun Luo[a], Zhen Ma[b,*], Liying Wang[c], Chengyun Huang[a], Yinghong Yue[a], Weiming Hua[a,*], Zi Gao[a]

[a] Shanghai Key Laboratory of Molecular Catalysis and Innovative Materials, Department of Chemistry, Fudan University, Shanghai 200433, PR China
[b] Shanghai Key Laboratory of Atmospheric Particle Pollution and Prevention (LAP^3), Department of Environmental Science and Engineering, Fudan University, Shanghai 200433, PR China
[c] Laboratory of Advanced Materials, Fudan University, Shanghai 200433, PR China

ARTICLE INFO

Article history:
Received 19 November 2014
Received in revised form 13 January 2015
Accepted 20 January 2015
Available online 21 January 2015

Keywords:
N_2O decomposition
CoZSM-11
CoZSM-5
Ion exchange
Stability

ABSTRACT

CoZSM-11 catalysts prepared using different methods (*i.e.*, wet ion exchange, buffered ion exchange, semi-continuous ion exchange, and impregnation) were tested in N_2O decomposition. For CoZSM-11 catalysts prepared by wet ion exchange, the activity increased with the decrease of the Si/Al ratio. Even higher activities can be achieved using catalysts prepared by buffered ion exchange or semi-continuous ion exchange. In contrast, CoZSM-11 prepared by impregnation was the least active. The catalysts were characterized by XRD, N_2 sorption, ICP, ^{27}Al MAS NMR, H_2-TPR, XPS, and UV–vis DRS. It was concluded that isolated Co^{2+} cations, in particular α-type Co^{2+}, were active sites, whereas the CoO_x species obtained by impregnation was much less active. The catalytic performance of CoZSM-11 and CoZSM-5 was compared as well.

1. Introduction

The anthropogenic generation of CO_x, NO_x, VOCs, ozone, and soot has attracted much concern recently because these substances are all air pollutants that may pollute the environment and cause health problems. With regard to NO_x, although much attention has been paid to NO (the most common pollutant among the NO_x family), N_2O still raises a lot of concern because it is a potent greenhouse gas with a global warming potential 310 times that of CO_2, and it also contributes to the ozone layer depletion [1–5] Anthropogenic N_2O comes from the combustion of fossil fuels and biomass, the production of nitric and adipic acids, the use of nitrogen fertilizers and so on [2]. Methods that have been used for the elimination of N_2O include thermal decomposition [5], non-selective catalytic reduction [2], selective catalytic reduction [6,7], and direct catalytic decomposition [1,8–10]. Among them, direct catalytic decomposition of N_2O ($N_2O = N_2 + 1/2\,O_2$) is the most efficient and economic.

Catalysts that have been explored in N_2O decomposition can be generally classified into supported noble metals [10–15], pure and mixed oxides [9,16–22], and zeolite-based catalysts [3,23–33]. Since Iwamoto et al. discovered that CuZSM-5 is useful in NO decomposition [34], many researchers have explored the application of Cu-based zeolites (*e.g.*, CuZSM-5 [35,36], CuBEA [37], CuMOR [38], CuSPAO-34 [39]) in N_2O decomposition. The preparation, characterization, and catalytic performance of CuZSM-5, together with the nature of active sites and reaction mechanisms, have been studied extensively [40–43].

Catalytic decomposition of N_2O over Co-based zeolites has been reported less frequently. da Cruz et al. found that CoZSM-5 prepared by ion exchange showed high activity in N_2O decomposition at 300 – 550 °C [44]. Liu et al. found that the catalytic activities of metal cation-exchanged BEA zeolites in N_2O decomposition followed the sequence of CoBEA > FeBEA > CuBEA, attributed to the different energy barriers for the desorption of O_2 [45]. Zhang et al. [46] ascribed the dramatically different activities of CoZSM-5, CoBEA, CoUSY, and CoMOR in N_2O decomposition to the presence of various kinds of Co species.

We recently found that CuZSM-11 was more active than CuZSM-5 in N_2O decomposition, due to the better accessibility of active species (Cu^+) and the weakened Cu^+—O bond [47]. It would be desirable to explore the catalytic application of ZSM-11 exchanged by other metal cations, and investigate the effect of preparation methods on the activity as well as the nature of active sites.

* Corresponding authors. Tel.: +86 21 65642409/2997; fax: +86 21 65641740.
E-mail addresses: zhenma@fudan.edu.cn (Z. Ma), wmhua@fudan.edu.cn (W. Hua).

http://dx.doi.org/10.1016/j.apcatb.2015.01.027
0926-3373/

The objective of the current work is to study the effect of preparation methods on the performance of CoZSM-11 in N_2O decomposition. It was found that the catalyst prepared by conventional ion exchange was much more active than the one prepared by impregnation, and the preparation of catalysts can be further optimized by using buffered ion exchange or semi-continuous ion exchange. The fact that CoZSM-11 catalysts prepared by different methods showed different catalytic activities provided us with an opportunity to investigate the nature of active sites.

2. Experimental

2.1. Catalyst preparation

NaZSM-11 samples with different Si/Al ratios were prepared hydrothermally [47]. $NaAlNO_2$ and NaOH were dissolved in aqueous tetrabutylammonium hydroxide (TBAOH), tetraethylorthosilicate was added, and the mixture was stirred till uniform. The molar composition of the gel was $4Na_2O{:}Al_2O_3{:}xSiO_2{:}20TBAOH{:}200H_2O$, where x was 30, 50, or 70. The gel was transferred into a Teflon lined autoclave and aged at 150 °C for 3 days. The product was filtered, washed, dried at 100 °C overnight and then calcined in air at 550 °C for 4 h. The obtained samples were exchanged in 1 M $NaNO_3$ solution at a solution/zeolite ratio of 10 mL g^{-1} at 80 °C for 4 h. The preparation of Co-containing catalysts by different methods is described below.

2.1.1. Wet ion exchange (WIE)

2.0 g NaZSM-11 (Si/Al = 15, 25, 36, as measured by X-ray fluorescence) were exchanged in 150 mL 0.01 M $Co(NO_3)_2$ solution at room temperature for 24 h. The ion exchanging procedure was repeated three times. The samples were filtered, washed, and dried at 100 °C overnight. The obtained samples are denoted as CoZSM-11WIE(Y), where Y represents the Si/Al ratio.

2.1.2. Buffered ion exchange (BUF)

CoZSM-11BUF(15) with a Si/Al ratio of 15 was prepared in a way similar to wet ion exchange described above [48]. The difference is that the $Co(NO_3)_2$ solution used for ion exchange was buffered at pH 8.0 by adding concentrated aqueous ammonia (28 wt%) slowly during the ion exchanging process.

2.1.3. Semi-continuous ion exchange (SMI)

CoZSM-11SMI(15) was prepared *via* semi-continuous ion exchange [49,50]. 2 g NaZSM-11 (Si/Al = 15) was mixed with 112.5 mL deionized water under stirring at 80 °C. 37.5 mL aqueous $Co(NO_3)_2$ (0.01 M) was added drop-wise at a rate of 1 mL min^{-1} at 80 °C. This ion-exchanging procedure was repeated three times. The sample was filleted, washed, and dried at 100 °C overnight.

2.1.4. Impregnation (IMP)

CoZSM-11IMP(15) was prepared by impregnating 2 g NaZSM-11 (Si/Al ratio = 15) with 9 mL aqueous $Co(NO_3)_2$ solution containing 0.248 g $Co(NO_3)_2$. The product was dried at 100 °C overnight, and then calcined in air at 550 °C for 4 h.

2.1.5. CoZSM-5SMI(15) prepared for comparison

NH_4ZSM-5 from Zeolyst (CBV3024E, Si/Al = 15, as measured by XRF) was calcined in static air at 450 °C for 4 h. The resulting HZSM-5 was exchanged in 1 M $NaNO_3$ solution with a solution/zeolite ratio of 10 mL g^{-1} at 80 °C for 4 h. The ion exchanging procedure was repeated three times. CoZSM-5SMI(15) was prepared in the same way as CoZSM-11SMI(15), using NaZSM-5 as the starting material.

2.2. Catalyst characterization

X-ray diffraction (XRD) experiments were conducted on a Bruker D8 Advance X-ray diffractometer using Ni-filtered Cu Kα radiation with a voltage and current of 40 kV and 40 mA, respectively. The bulk Si/Al ratios of zeolites were measured by XRF on a Bruker-AXS S4 Explorer instrument. The Co and Al contents were determined by inductively coupled plasma (ICP) atomic emission spectroscopy using a Thermo Electron IRIS Intrepid II XSP spectrometer after dissolution of samples in aqueous HF. The BET surface areas and micropore volumes of samples were analyzed by N_2 sorption at −196 °C using a Micromeritics ASAP 2010 instrument.

^{27}Al magic-angle spinning nuclear magnetic resonance (^{27}Al MAS NMR) characterization was performed on a Bruker DSX-300 spectrometer at a resonance frequency of 104.3 MHz and a spinning rate of 12 kHz. The samples were hydrated in a desiccator over a saturated NaCl solution for 3 days prior to the measurements.

Temperature-programmed reduction (TPR) profiles were obtained on a Micromeritics AutoChem II apparatus using 0.1 g sample. The samples were pretreated in He at 500 °C for 2 h, cooled to 50 °C in He, contacted with a H_2/Ar mixture (10 vol.% H_2) flowing at 30 mL min^{-1}, and heated at a ramping rate of 10 °C min^{-1} to 950 °C. The H_2 consumption was monitored using a thermal conductivity detector (TCD).

X-ray photoelectron spectroscopy (XPS) data were obtained on a Shimadzu/Kratos Axis ultradld spectrometer with Al Kα radiation as the excitation source. Before the measurements, the samples were pretreated in He at 500 °C for 2 h. The adventitious carbonaceous C 1s line (284.6 eV) was used to calibrate the binding energy (BE). The XPS spectra were deconvoluted with Shirley background subtraction and a Gaussian/Lorenzian ratio of 70/30.

Diffuse reflectance Ultraviolet–visible (UV–vis) spectra were recorded on a Shimadzu UV-2450 spectrometer using $BaSO_4$ as the reference. Before the measurements, the samples were pretreated in He at 500 °C for 2 h. The UV–vis data were deconvoluted into Gaussian-type peaks using Origin 9.0 software, according to the peak assignments and procedure reported in the literature [51–53].

2.3. Catalytic tests

Catalytic decomposition of N_2O was conducted in a fixed-bed flow reactor at atmospheric pressure [54]. Briefly, 0.2 g catalyst (40–60 meshes) was loaded into a U-shaped glass tube (7 mm i.d.), heated to 500 °C at a rate of 10 °C min^{-1} under flowing He (50 mL min^{-1}), and held at 500 °C for 2 h. After cooling down to room temperature, 0.5% N_2O/He (60 mL min^{-1}) flowed through the catalyst for 1 h, during which the concentration of N_2O were periodically measured by GC (Agilent 7890 A) with a TCD detector. The reaction temperature was then varied using a furnace and kept at various elevated temperatures for 30 min in each temperature step. The existing stream was again periodically analyzed by the GC, and the conversion of N_2O was calculated according to $X = ([N_2O]_{in} - [N_2O]_{out})/[N_2O]_{in}$, where $[N_2O]_{in}$ refers to the N_2O concentration at room temperature, and $[N_2O]_{out}$ refers to the N_2O concentration at an elevated temperature.

To study the effect of O_2 or H_2O on the catalytic activities of CoZSM-11SMI(15) and CoZSM-5SMI(15), 5% O_2 or 2% H_2O was added into the reaction mixture whereas the concentration of N_2O was still 0.5%, and the total flow rate of the reaction mixture was still 60 mL min^{-1}.

To test the stability of CoZSM-11SMI(15) and CoZSM-5SMI(15), the N_2O conversions were measured as a function of time on stream. After pretreatment in He at 500 °C for 2 h, the catalyst was kept at 500 °C. The ambient was switched to the reactant gas (0.5% N_2O, 2% H_2O, balance He) and the exiting stream was periodi-

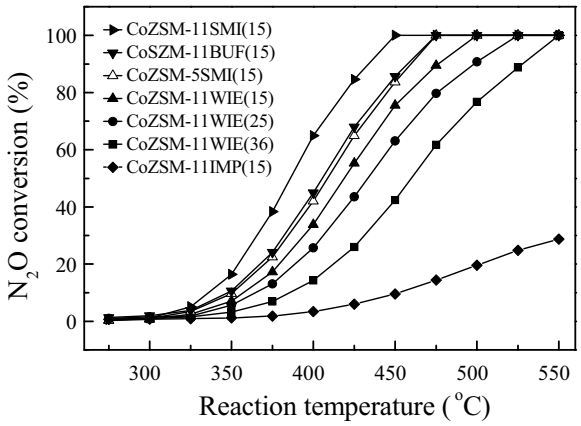

Fig. 1. Conversion of N_2O over (►) CoZSM-11SMI(15), (◄) CoZSM-11BUF(15), (▼) CoZSM-5SMI(15), (▲) CoZSM-11WIE(15), (●) CoZSM-11WIE(25), (■) CoZSM-11WIE(36), and (♦) CoZSM-11IMP(15). Conditions: 0.5% N_2O, balance He.

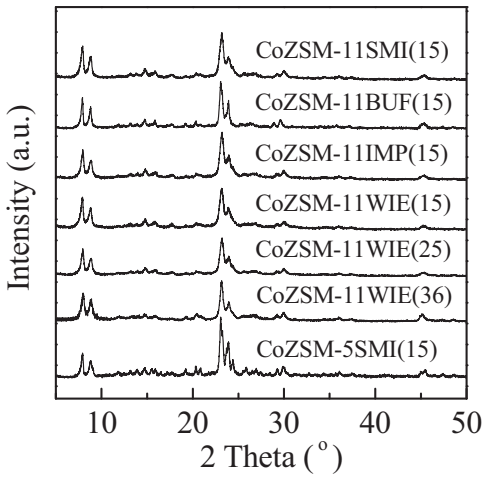

Fig. 2. XRD patterns of different samples.

cally analyzed by GC for 100 h. Finally, the catalyst was cooled down while the gas stream was still flowing. The $[N_2O]_{in}$ was obtained when the catalyst was cooled and no N_2O decomposition took place.

3. Results

3.1. Catalytic decomposition of N_2O

Fig. 1 shows the N_2O conversions obtained using different CoZSM-11 catalysts, as a function of reaction temperature. These catalysts are not active below 325 °C, and they start to show some activities above 325 or 350 °C. For CoZSM-11WIE catalysts with different Si/Al ratios, the N_2O conversions over CoZSM-11WIE(15), CoZSM-11WIE(25), and CoZSM-11WIE(36) at 450 °C are 75.5%, 63.0%, and 42.4% respectively, being the highest when the Si/Al ratio of ZSM-11 is 15.

We also prepared CoZSM-11 catalysts with the same Si/Al ratio of 15, by buffered ion exchange (BUF), semi-continuous ion exchange (SMI), and impregnation (IMP) methods. As shown in Fig. 1, the catalysts prepared by BUF and SMI are more active than the one prepared by WIE mentioned above, whereas the catalyst prepared by IMP is the least active. The N_2O conversions over CoZSM-11SMI(15), CoZSM-11BUF(15), CoZSM-11WIE(15), and CoZSM-11IMP(15) at 400 °C are 64.9%, 44.9%, 33.8%, and 3.4%, respectively.

To set the results in context, we additionally prepared CoZSM-5SMI(15) by SMI. As shown in Fig. 1, CoZSM-11SMI(15) is more active than CoZSM-5SMI(15). The N_2O conversions over these catalysts at 400 °C are 64.9% and 42.1%, respectively.

Because the Co contents of these catalysts are not exactly the same, in particular for those with different Si/Al ratios (Table 1), we computed the specific rates (expressed as moles of N_2O converted per mole of Co per hour) achieved at 375 °C. As shown in Table 1, the specific rates of CoZSM-11 catalysts prepared by WIE increases from 1.17 to 1.25 then to 1.40 h^{-1} when the Si/Al ratio decreases from 36 to 25 and then to 15. CoZSM-11SMI(15) and CoZSM-11BUF(15) show higher specific rates of 2.31 and 1.60 h^{-1}, respectively, whereas CoZSM-11IMP(15) shows the lowest specific rate of 0.10 h^{-1}. In addition, CoZSM-11SMI(15) with a specific rate of 2.31 h^{-1} is more active than CoZSM-5SMI(15) with a specific rate of 1.54 h^{-1}.

3.2. Basic physicochemical properties

Fig. 2 shows the XRD patterns of samples. CoZSM-11 samples, regardless of the Si/Al ratio and preparation methods, all exhibit characteristic peaks assigned to ZSM-11. On the other hand, CoZSM-5 shows characteristic peaks corresponding to ZSM-5. The differences between two kinds of zeolites are distinguished in the 2θ ranges of 22.5–25.0° and 44.5–46.0° [55]. For instance, in the 2θ range of 22.5–25.0°, ZSM-5 exhibits five characteristic peaks indexed to the (5 0 1), (0 5 1), (1 5 1), (3 0 3), and (1 3 3) crystal planes, whereas ZSM-11 has two peaks corresponding to the (5 0 1) and (3 0 3) planes.

Table 1 collects additional data on the physicochemical properties. As shown in Table 1, the bulk Si/Al ratios of ZSM-11 zeolites measured by XRF is close to those of the initial gels. The BET surface areas of CoZSM-11 samples are in the range of 336–358 $m^2\ g^{-1}$,

Table 1
Chemical composition and textural properties of different samples.

Sample	Si/Al molar ratio		Co/Al[c]	Co[c]	S_{BET}	V_{micro}[d]	V_{meso}	Specific rate[e]
	Gel[a]	Bulk[b]	molar ratio	(wt%)	($m^2\ g^{-1}$)	($cm^3\ g^{-1}$)	($cm^3\ g^{-1}$)	(h^{-1})
CoZSM-11SMI(15)	15	15	0.52	3.59	351	0.13	0.058	2.31
CoZSM-11BUF(15)	15	15	0.45	3.08	340	0.13	0.078	1.60
CoZSM-11IMP(15)	15	15	0.58	3.79	336	0.13	0.057	0.10
CoZSM-11WIE(15)	15	15	0.41	2.67	347	0.13	0.059	1.40
CoZSM-11WIE(25)	25	25	0.43	2.25	358	0.13	0.061	1.25
CoZSM-11WIE(36)	35	36	0.41	1.27	345	0.13	0.059	1.17
CoZSM-5SMI(15)	–	15	0.56	3.62	367	0.13	0.096	1.54

[a] Calculated from the amounts of $Si(OC_2H_5)_4$ and $NaAlO_2$ added in the reactant gel.
[b] Determined by XRF.
[c] Determined by ICP.
[d] Calculated by *t*-plot method.
[e] Moles of N_2O converted per mole of Co per hour at 375 °C.

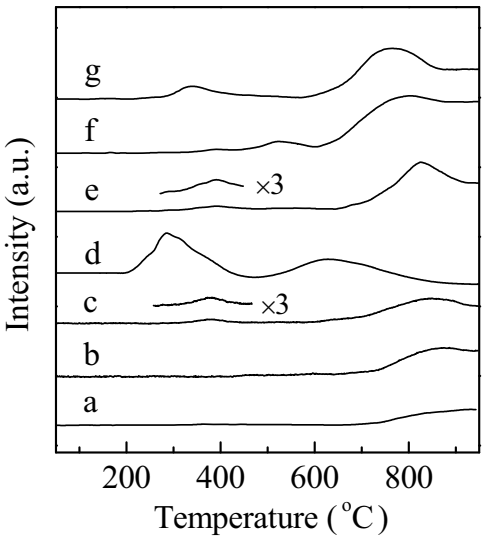

Fig. 3. H_2-TPR profiles of (a) CoZSM-11WIE(36), (b) CoZSM-11WIE(25), (c) CoZSM-11WIE(15), (d) CoZSM-11IMP(15), (e) CoZSM-11BUF(15), (f) CoZSM-5SMI(15), and (g) CoZSM-11SMI(15).

whereas CoZSM-5 has a surface area of 367 $m^2\,g^{-1}$, *i.e.*, the difference among the surface areas of these samples is within 10%. The microporous volumes of all the CoZSM-11 samples are 0.13 $cm^3\,g^{-1}$. The mesoporous volumes of most of the CoZSM-11 samples are about 0.06 $cm^3\,g^{-1}$, except that the microporous volume of CoZSM-11BUF(15) is 0.78 $cm^3\,g^{-1}$. The increment of mesoporous volume for CoZSM-11BUF(15) may be because the basic environment (pH 8) during the ion exchanging process facilitates the creation of some mesopores.

A more important parameter is the Co content. The Co contents (2.67 wt%, 2.25 wt%, 1.27 wt%) of CoZSM-11WIE samples decrease as the Si/Al ratio (15, 25, 36) increases. In zeolites, the negative charges of ≡Al—O—Si≡ bridges are balanced by Na^+ or H^+ cations, so the amount of Co^{2+} that can exchange with Na^+ or H^+ on ion-exchange sites of zeolites is related to the amount of framework Al, *i.e.*, the Si/Al ratio. The Co/Al molar ratios of these three samples are measured to be 0.41–0.43, corresponding to ca. 80% of the cation exchange capacity.

Higher Co/Al ratios (0.45, 0.52) and Co loadings (3.08 wt%, 3.59 wt%) can be achieved on CoZSM-11BUF(15) and CoZSM-11SMI(15). The high Co content in CoZSM-11BUF(15) can be explained by the conversion of ca. 50% Co^{2+} into $[Co(OH)]^+$ when the pH value of the aqueous solution used for ion exchange is adjusted to 8 [56]. $[Co(OH)]^+$ may exchange with Na^+ or H^+ cations that compensate the ≡Al—OH—Si≡ bridges on the zeolite more easily than Co^{2+} [56]. The high Co content in CoZSM-11SMI(15) can be explained by the high ion exchange temperature (80 °C).

3.3. H_2-TPR

The catalysts were *in situ* pretreated in He at 500 °C for 2 h (the same pretreatment condition as used in catalytic tests) before H_2-TPR. As shown in Fig. 3, up to three reduction regions can be distinguished. In reference to the literature [48,57–59], a peak at 700–950 °C can be assigned to the reduction of mono-atomic Co^{2+} at ion-exchange sites, a peak at 200–400 °C can be ascribed to the reduction of Co_3O_4 located at the external surface of zeolite, whereas an additional weak peak at 400–700 °C corresponds to the reduction of CoO_x.

For CoZSM-11WIE catalysts with different Si/Al ratios (Fig. 3a–c), the reduction peak corresponding to mono-atomic Co^{2+} is always present, and a weak reduction peak corresponding to Co_3O_4 appears when the Si/Al ratio decreases to 15 (*i.e.*, the Co content increases). For CoZSM-11 samples prepared by different methods (Fig. 3d, e, and g), mono-atomic Co^{2+} and small portions of Co_3O_4 are both present on the most active CoZSM-11BUF(15) and CoZSM-11SMI(15), whereas the least active CoZSM-11IMP(15) has predominantly Co_3O_4 and CoO_x. In addition, CoZSM-5SMI(15) has predominately mono-atomic Co^{2+} and a small fraction of CoO_x. Thus, we may conclude that isolated Co^{2+} cations are the main active species in N_2O decomposition, whereas Co_3O_4 or CoO_x exhibit much lower activity.

Table 2
H_2-TPR results of different catalysts.

Catalyst	Peak temperature (°C)			H_2 uptake (mmol g^{-1})		
	I	II	III	I	II	III
CoZSM-11SMI(15)	338	–	765	0.033	–	0.584
CoZSM-11BUF(15)	392	–	826	0.010	–	0.521
CoZSM-11IMP(15)	286	628	–	0.403	0.341	–
CoZSM-11WIE(15)	376	–	849	0.008	–	0.430
CoZSM-11WIE(25)	–	–	874	–	–	0.365
CoZSM-11WIE(36)	–	–	940	–	–	0.216[a]
CoZSM-5SMI(15)	–	521	804	–	0.026	0.590

[a] Calculated according to the result of ICP.

For CoZSM-11WIE catalysts, the reduction peak temperature of mono-atomic Co^{2+} shifts toward lower temperatures as the Si/Al ratio decreases (Fig. 3 and Table 2), *i.e.*, a lower reduction temperature of mono-atomic Co^{2+} correlates to the high activity of the catalyst. The reduction peak temperatures of Co^{2+} on CoZSM-11SMI(15), CoZSM-11BUF(15), and CoZSM-11WIE(15) are 765, 826, and 849 °C, respectively, again correlating nicely with the trend seen in activity tests. For comparison, the reduction peak temperatures of Co^{2+} on CoZSM-11SMI(15) and CoZSM-5SMI(15) are 765 and 804 °C, again consistent with the activity trend. The lower reduced peak temperature means the weaker strength of the Co^{2+}—O bond, which could facilitate the decomposition of N_2O [47,60]. As seen in Table 2, the H_2 consumption of Co^{2+} species decreases with the increase of the Si/Al ratio, and increases with the increase of the Co loading. In addition, CoZSM-11SMI(15) and CoZSM-5SMI(15) possess the equivalent amount of Co^{2+}.

3.4. XPS

CoZSM-11 and CoZSM-5SMI(15) pretreated in He at 500 °C for 2 h were examined by XPS. Fig. 4 shows two major binding energy features around 782 and 798 eV corresponding to Co $2p_{3/2}$ and Co $2p_{1/2}$, respectively [61,62]. Two satellite peaks (around 787 and 803 eV) are also observed at higher binding energies, confirming the existence of Co^{2+}. In reference to previous XPS results [61–63], the $2p_{3/2}$ main peak for CoZSM-11 was deconvoluted into a Co^{2+} peak at about 781.7 eV and a smaller peak for Co oxide at about 780.7 eV. A similar peak-fitting analysis for CoZSM-5SMI(15) resulted in the deconvolution of the $2p_{3/2}$ main peak into a Co^{2+} peak at 782.1 eV and a smaller peak for Co oxide at 781.0 eV. The fitted results and the area ratios of Co oxide/Co^{2+} are summarized in Table 3. Here Co^{2+} refers to Co^{2+} located at ion-exchange positions of zeolites [61], whereas cobalt oxide may potentially be CoO [64], Co_3O_4 [65,66], or Co_2O_3 [67]. In reference to the H_2-TPR results, we verify that the cobalt oxide species on CoZSM-11 is mainly Co_3O_4, and that on CoZSM-5 is CoO_x.

As shown in Fig. 4 and Table 3, CoZSM-11WIE(25) and CoZSM-11WIE(36) show the dominant presence of Co^{2+} species, as seen from the fact that the Co $2p_{3/2}$ peaks for these catalysts are both at 781.7 eV. With the decrease in Si/Al ratio to 15 and the increase of Co loading, Co oxide appears. Considering the difference of preparation methods (ion-exchange *vs.* impregnation), CoZSM-11IMP(15)

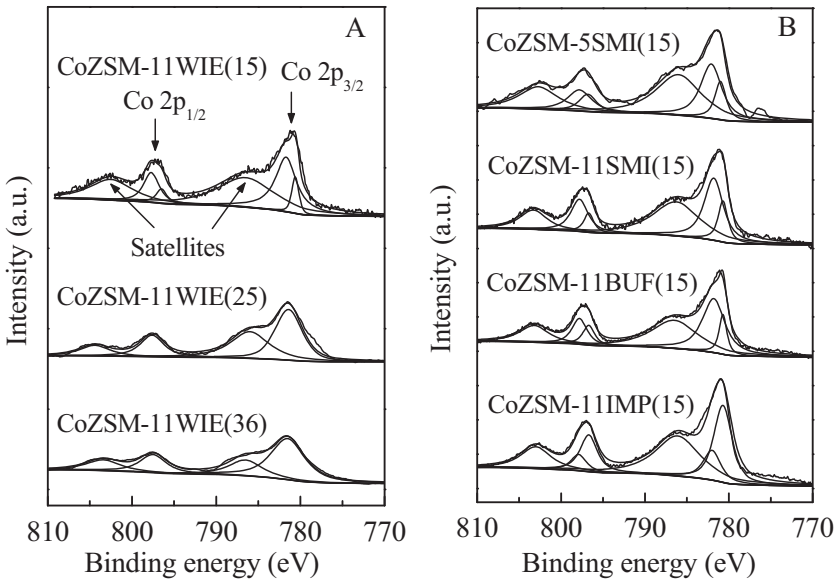

Fig. 4. XPS spectra of the Co 2p region for CoZSM-11 and CoZSM-5SMI(15) samples. (A) CoZSM-11WIE(15), CoZSM-11WIE(25), CoZSM-11WIE(36); (B) CoZSM-5SMI(15), CoZSM-11SMI(15), CoZSM-11BUF(15), CoZSM-11IMP(15).

Table 3
XPS data of CoZSM-11 and CoZSM-5SMI(15) samples.

Sample	Binding energy (eV)		Co oxide/Co^{2+}
	Co oxide $2p_{3/2}$	Co^{2+} $2p_{3/2}$	
CoZSM-11SMI(15)	780.7	781.8	0.34
CoZSM-11BUF(15)	780.7	781.8	0.25
CoZSM-11IMP(15)	780.7	781.8	2.50
CoZSM-11WIE(15)	780.6	781.7	0.18
CoZSM-11WIE(25)	–	781.6	0
CoZSM-11WIE(36)	–	781.6	0
CoZSM-5SMI(15)	781.0	782.1	0.38

has more Co oxide and less Co^{2+}, whereas the CoZSM-11 samples prepared by ion exchange methods have more Co^{2+}, consistent with the H_2-TPR data.

By comparing the fitted results for CoZSM-11SMI(15) and CoZSM-5SMI(15) (Fig. 4B, Table 3), we can find that the two samples have similar Co oxide/Co^{2+} area ratios, whereas the binding energy of Co^{2+} on CoZSM-5SMI(15) (782.1 eV) is higher than that on CoZSM-11SMI(15) (781.8 eV). This implies that Co^{2+} in CoZSM-11SMI(15) could be reduced more readily [68,69], consistent with the H_2-TPR data reported above.

3.5. UV–vis DRS spectra of CoZSM-11 samples and CoZSM-5SMI(15)

Results from the H_2-TPR and XPS characterization have proven the Co^{2+} as the active site for N_2O decomposition. The Co ions located at different sites of the zeolites may coordinate differently to the framework oxygen and perturb the framework oxygen to different extents. These properties may influence catalytic activities [70]. Therefore, UV–vis DRS, an effective technique to analyze different Co species [52,53,71–73], was employed to characterize different Co-containing zeolites.

The UV–vis DRS spectra of the CoZSM-11 catalysts and CoZSM-5SMI(15) are shown in Fig. 5. The strong absorbance in the region of 12,500–27,500 cm^{-1} reveals the existence of various Co^{2+} species in Co-based zeolites prepared by ion exchange. Several characteristic bands attributed to specific isolated Co^{2+} located at the typical cationic sites (referred to as α, β and γ) can be deconvoluted. According to the literature [46,52,62], the band at about 15,400 cm^{-1} corresponds to α-type Co^{2+} situated in the straight, 10-membered ring channels. Four bands at around 16,500, 18,200, 19,300, 21,800 cm^{-1} are assigned to β-type Co^{2+} located at the intersection of the channels. Two bands at 20,430 and 23,020 cm^{-1} belong to γ-type Co^{2+} coordinated to framework oxygen in the opening of so called "boat-shaped" sites. All of these bands of different Co^{2+} cations (15,400, 16,500, 18,200, 19,300, 21,800, 20,430, and 23,020 cm^{-1}) are ascribed to the $^4A_2(F) \rightarrow {}^4T_1(P)$ transition [74]. The bands at around 13,700 cm^{-1} and the broad band at 20,000–26,000 cm^{-1} are typical for Co_3O_4 particles, and they are ascribed to octahedral Co^{3+} ($^1A_{1g} \rightarrow {}^1T_{1g}$ and $^1A_{1g} \rightarrow {}^1T_{2g}$ transitions) [75,76]. A band at 19,330 cm^{-1} is attributed to $^1T_{1g}(F) \rightarrow {}^1T_{1g}(P)$ transition and indicative of CoO_x clusters [59].

The distribution of individual Co^{2+} types and other Co oxides in all catalysts was analyzed quantitatively by calculating the integral intensities of their spectral bands and listed in Table 4. The results reveal that (i) the bands corresponding to isolated Co^{2+} are stronger for catalysts prepared by ion exchange, whereas CoZSM-11IMP(15) presents the strongest bands corresponding to Co_3O_4 and CoO_x species; (ii) as for isolated Co^{2+} in ion exchanged samples, the most populated site is the β-type Co^{2+} (71–88%), followed by α-type Co^{2+} (8–16%) and the least populated γ-type Co^{2+} (1–10%). CoZSM-11SMI(15) has more α-type Co^{2+} than CoZSM-5SMI(15), although these two catalysts have equivalent amount of Co^{2+}. (iii) For CoZSM-11 samples prepared by ion exchange, the population of α-type Co^{2+} increases with the increase of the Co loading, whereas the population of β-type Co^{2+} decreases with the increase of the Co loading. In contrast, the concentrations of the γ-type Co^{2+} are relatively lower. These results imply that different preparation methods may influence the distribution of these specific Co ions.

Fig. 6 correlates the specific rate (as activity per Co) at 375 °C to Co ions at different cationic sites (α, β, and γ). Interestingly, the specific rates of different catalysts correlate with the concentrations of α-type Co^{2+} in different catalysts, indicating the α-type Co^{2+} sites are the most active in all samples.

3.6. The effect of O_2 and H_2O

The effect of O_2 and/or H_2O on the catalytic activity of CoZSM-11SMI(15) and CoZSM-5SMI(15) was investigated. As shown in

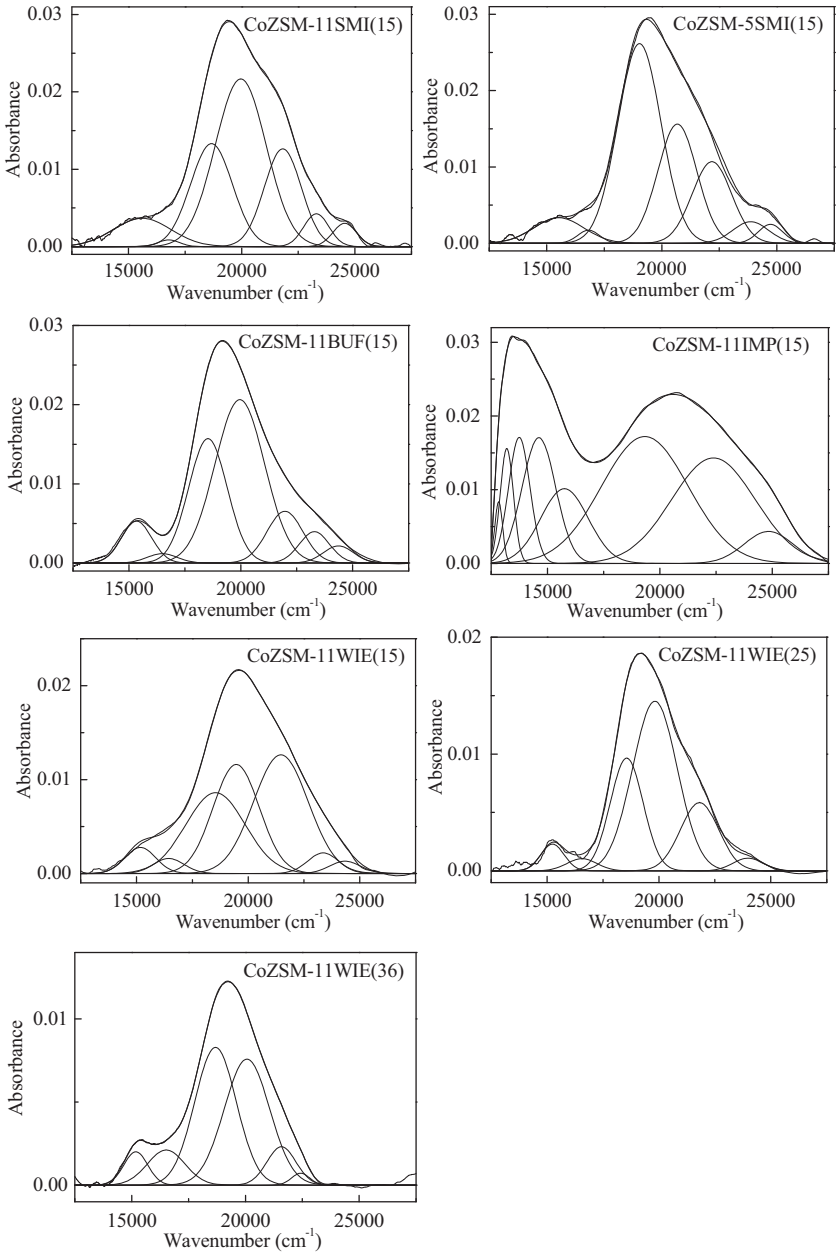

Fig. 5. UV–vis DRS spectra of CoZSM-11 and CoZSM-5SMI(15) samples.

Fig. 7, the addition of 5% O_2 to 0.5% N_2O has no obvious effect on the catalytic activity of both catalysts. In the literature, CoZSM-5 was found to be O_2-resistent [44,48,56,77]. On the other hand, the addition of 2% H_2O has an inhibiting effect. For instance, the N_2O conversions over CoZSM-11SMI(15) and CoZSM-5SMI(15) at 400 °C are 64.9% and 42.1%, respectively, in the absence of H_2O, whereas the N_2O conversions decrease to 12.7% and 3.9%, respectively, in the presence of H_2O. The negative effect of H_2O is commonly attributed

Table 4
Percentage of deconvoluted band areas and the corresponding Co species loadings.

Catalyst	I_α[a] (%)	I_β[a] (%)	I_γ[a] (%)	I_{Co2+}[a] (%)	I_{Co3O4}[a] (%)	I_{CoOx}[a] (%)	Co_α[b] (wt%)	Co_β[b] (wt%)	Co_γ[b] (wt%)	Co^{2+}[b] (wt%)	Co_3O_4[b] (wt%)	CoO_x[b] (wt%)
CoZSM-11SMI(15)	16.08	71.71	9.52	97.31	2.69	0.00	0.58	2.57	0.34	3.49	0.13	0.00
CoZSM-11BUF(15)	12.78	74.95	9.86	97.59	2.41	0.00	0.39	2.31	0.31	3.01	0.10	0.00
CoZSM-11IMP(15)	0.00	4.99	1.02	6.01	42.76	51.23	0.00	0.19	0.04	0.23	2.21	2.47
CoZSM-11WIE(15)	9.95	87.04	2.31	99.30	0.70	0.00	0.27	2.32	0.06	2.65	0. 03	0.00
CoZSM-11WIE(25)	8.05	88.14	3.81	100	0.00	0.00	0.18	1.98	0.09	2.25	0.00	0.00
CoZSM-11WIE(36)	8.17	88.28	3.55	100	0.00	0.00	0.10	1.12	0.05	1.27	0.00	0.00
CoZSM-5SMI(15)	10.01	74.55	10.62	95.18	0.00	4.82	0.36	2.70	0.39	3.45	0.00	0.22

[a] Calculated from the data in Fig. 5.
[b] Calculated from the data in Fig. 5 and the result of ICP. The loading of CoO_x was calculated in terms of CoO.

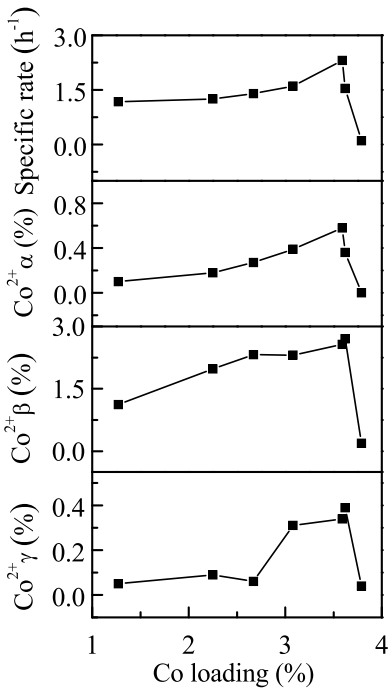

Fig. 6. The correlations of specific rates and the concentrations of the α-, β-, and γ-type Co^{2+} in Co-containing zeolites.

to the competitive adsorption between N_2O and H_2O, and sometimes to the migration of isolated Co^{2+} induced by H_2O [78].

3.7. Reaction order of N_2O over CoZSM-11SMI(15)

Kapteijn et al. [79] reported that N_2O decomposition over CoZSM-5 follows an Eley–Rideal mechanism with a first order in N_2O. Here we recorded the conversions of N_2O over CoZSM-11SMI(15) at 330 °C, as a function of N_2O inlet concentration. The conversion data and the corresponding rates are given in Table S1 in the Supporting information. In Fig. S1, the ln(rate) *vs.* ln(N_2O conc.) is plotted, from which the reaction order of N_2O can be obtained. At 330 °C, a first order in N_2O is observed. The reaction mechanism will be studied in more detail in the future.

3.8. Stability of CoZSM-11SMI(15) and CoZSM-5SMI(15)

The stability of CoZSM-11SMI(15) and CoZSM-5SMI(15) in N_2O decomposition in the presence of 2% H_2O was studied. As shown in

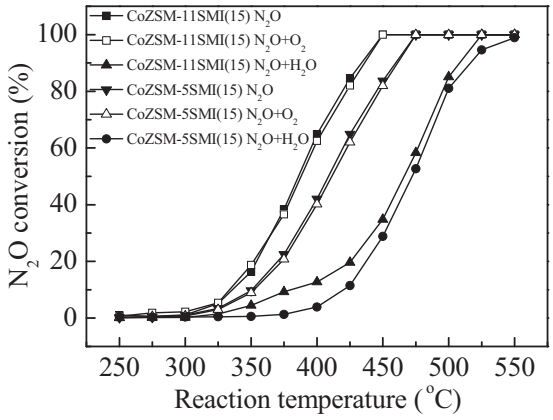

Fig. 7. The influences of co-feed 5% O_2 and/or 2% H_2O on the conversion of N_2O over CoZSM-11SMI(15) and CoZSM-5SMI(15).

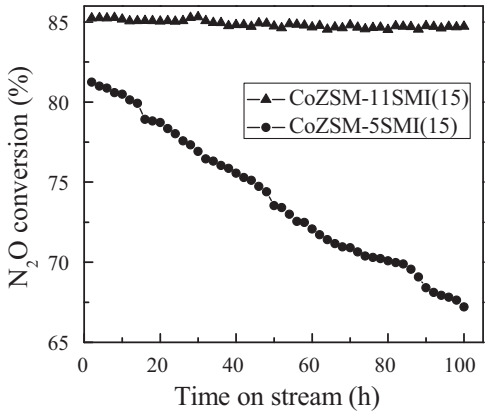

Fig. 8. Conversion of N_2O over CoZSM-11SMI(15) and CoZSM-5SMI(15) as a function of time on stream. Conditions: 0.5% N_2O, 2% H_2O, balance He.

Fig. 8, the N_2O conversion over CoZSM-11SMI(15) at 500 °C maintains at ca. 85% in 100 h. In contrast, the N_2O conversion over CoZSM-5SMI(13) decreased gradually with time on stream, from the initial 81.2% to 67.2% after 100 h.

CoZSM-11SMI(15) and CoZSM-5SMI(15) collected before and after the stability tests were characterized by ^{27}Al MAS NMR. As shown in Fig. 9, only an intense signal at 56 ppm (assigned to framework Al in tetrahedral coordination [80,81]) is observed for CoZSM-11SMI(15), either before or after the stability test (Fig. 9c and d), indicating that no dealumination occurs. For comparison, in addition to an intense signal at 56 ppm, another signal at 0 ppm attributed to extra-framework Al in octahedral coordination [80,81] can be found for CoZSM-5SMI(15) either before or after the stability test (Fig. 9a and b). The fraction of extra-framework Al atoms in CoZSM-5SMI(15) collected after the stability test (7.1%) is higher than that of CoZSM-5SMI(15) before the stability test (1.4%), indicating the occurrence of dealumination [82]. Additionally, the chemical shift of framework Al in the spent CoZSM-5SMI(15) shifts slightly from 55.4 to 54.5 ppm, again caused by dealumination [82].

UV–vis DRS was used to characterize CoZSM-11SMI(15) and CoZSM-5SMI(15) collected before and after the stability tests, and the results are shown in Fig. S2 and Table S2. As seen in Table S2, the amounts of Co^{2+} and Co_3O_4 in CoZSM-11SMI(15) collected after the stability test are similar to the corresponding values in the catalyst before the stability test. However, for CoZSM-5SMI(15) collected before and after the stability test, the amounts of Co^{2+} are 3.45–3.13 wt%, whereas the amount of CoO_x are 0.22–0.59 wt%, respectively, implying the transformation of some framework Co^{2+}

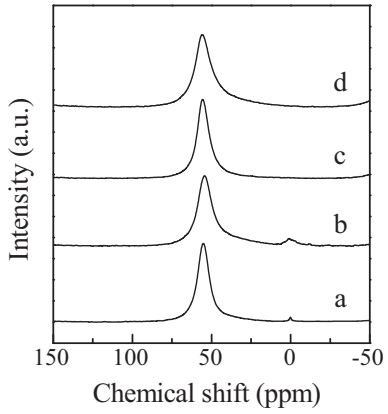

Fig. 9. ^{27}Al NMR spectra of (a) CoZSM-5SMI(15) collected before the stability test, (b) CoZSM-5SMI(15) collected after the stability test, (c) CoZSM-11SMI(15) collected before the stability test, and (d) CoZSM-11SMI(15) collected after the stability test.

into Co oxide. This observation explains the different stability patterns of CoZSM-11SMI(15) and CoZSM-5SMI(15).

4. Discussion

Among CoZSM-11WIE catalysts with different Si/Al ratios (Si/Al = 15, 25, 36), the most active catalyst is the one with a Si/Al ratio of 15 (Fig. 1, Table 1), because it contains more Co^{2+} active for N_2O decomposition. In addition, the catalytic activities of CoZSM-11 catalysts prepared by different methods correlate to the amounts of Co^{2+} in these catalysts, whereas Co oxides in CoZSM-11IMP(15) are the least active. In a report on N_2O decomposition over Co-MFI and Co-MOR zeolites, mono-atomic Co^{2+} was found to be much more active than Co oxide [46].

It is generally accepted that Co ions are located at different ion-exchange sites of zeolites, and their distribution greatly influences the activity in N_2O decomposition [3,62]. UV–vis DRS data show that, for CoZSM-11 prepared by various ion exchange methods, the most populated site is β-type Co^{2+}, followed by α-type Co^{2+} and the least populated γ-type Co^{2+}. The preparation methods influence the distribution of the specific Co^{2+} sites, and the higher Co content favors the increase of the population of α-type Co^{2+}. As shown in Fig. 6, the specific rates correlate with the concentration of α-type Co^{2+}, indicating the α-type Co^{2+} sites are the most active. In ZSM-11, the α-type Co^{2+} sites are coordinated to the rectangle of four framework oxygen atoms in the straight channel. This site is composed of two folded five-membered rings forming an enlongated six-membered ring. Their favorite location is easily accessible to reactants and intermediates, and they exhibit the weakest bonding to framework oxygen among the individual Co ions [53,73]. However, the β-type Co^{2+} sites are coordinated closely to the plane of the deformed six-membered ring in the intersections of straight channels, and therefore, are less accessible compared to the α-type Co^{2+} sites. Moreover, β-type Co^{2+} sites bind to framework oxygen atoms more strongly than α-type Co^{2+}, thus making the electron-donating molecule N_2O less readily coordinate to β-type Co^{2+} [53,73].

CoZSM-11SMI(15) is more active than CoZSM-5SMI(15) with comparable Co content and amount of active Co^{2+} (Fig. 1, Table 1). Characterization by H_2-TPR and XPS has confirmed that the Co^{2+}—O bond on CoZSM-11SMI(15) is weaker than on CoZSM-5SMI(15). This is considered to be one reason responsible for the superior activity of CoZSM-11SMI(15) than CoZSM-5SMI(15). The micropore sizes of ZSM-11 and ZSM-5 zeolites are similar, *i.e.*, about 0.55 nm. However, ZSM-11 only has straight channels, whereas ZSM-5 consists of both straight channels and sinusoidal channels [83,84]. The α-type Co^{2+} sites are coordinated to the rectangle of four framework oxygen atoms in the straight channel. UV–vis DRS data show that CoZSM-11SMI(15) has more α-type Co^{2+} than CoZSM-5SMI(15), consistent with the higher activity achieved on CoZSM-11SMI(15).

5. Conclusions

A series of CoZSM-11 catalysts were prepared by different methods and tested in N_2O decomposition. The N_2O conversion and specific rate of CoZSM-11 prepared by wet ion exchange increase with the decrease in Si/Al ratio. The activity can be further enhanced when synthesizing the catalyst by buffered ion exchange or semi-continuous ion exchange, whereas the catalyst prepared by impregnation shows the lowest activity. H_2-TPR, XPS and UV–vis DRS characterizations indicate that Co^{2+} ions are the main active sites for N_2O decomposition. The sequence of activity is a consequence of the increased amount of active Co^{2+} species as well as the weakened Co^{2+}—O bond. Moreover, the α-type Co^{2+} ions coordinated to framework oxygen atoms are indicated to the most active sites. CoZSM-11 is found to be more active and stable than CoZSM-5 for N_2O decomposition.

Acknowledgments

W. Hua and Y. Yue thank the financial support by the National Natural Science Foundation of China (20773027 and 21273043) and the Science and Technology Commission of Shanghai Municipality (13DZ2275200). Z. Ma thanks the financial support by the National Natural Science Foundation of China (21477022). Y. Luo thanks the financial support by National Fund for Talent Training in Basic Science (J1103304).

Appendix A. Supplementary data

Supplementary data associated with this article can be found, in the online version, at http://dx.doi.org/10.1016/j.apcatb.2015.01.027.

References

[1] F. Kapteijn, J. Rodriguez-Mirasol, J.A. Moulijn, Appl. Catal. B 9 (1996) 25–64.
[2] J. Perez-Ramirez, F. Kapteijn, K. Schoffel, J.A. Moulijn, Appl. Catal. B 44 (2003) 117–151.
[3] B.M. Abu-Zied, W. Schwieger, A. Unger, Appl. Catal. B 84 (2008) 277–288.
[4] N. Imanaka, T. Masui, Appl. Catal. A 431 (2012) 1–8.
[5] M. Galle, D.W. Agar, O. Watzenberger, Chem. Eng. Sci. 56 (2001) 1587–1595.
[6] G. Centi, F. Vazzana, Catal. Today 53 (1999) 683–693.
[7] S. Kameoka, K. Kita, T. Takeda, S. Tanaka, S. Ito, K. Yuzaki, T. Miyadera, K. Kunimori, Catal. Lett. 69 (2000) 169–173.
[8] A. Dandekar, M.A. Vannice, Appl. Catal. B 22 (1999) 179–200.
[9] J. Perez-Ramirez, J. Overeijnder, F. Kapteijn, J.A. Moulijn, Appl. Catal. B 23 (1999) 59–72.
[10] X.D. Xu, H.L. Xu, F. Kapteijn, J.A. Moulijn, Appl. Catal. B 53 (2004) 265–274.
[11] S. Kawi, S.Y. Liu, S.C. Shen, Catal. Today 68 (2001) 237–244.
[12] S. Parres-Esclapez, I. Such-Basanez, M.J. Illan-Gomez, C.S.M. de Lecea, A. Bueno-Lopez, J. Catal. 276 (2010) 390–401.
[13] I. Mejia-Centeno, S. Castillo, G.A. Fuentes, Appl. Catal. B 119 (2012) 234–240.
[14] M. Konsolakis, I.V. Yentekakis, G. Pekridis, N. Kaklidis, A.C. Psarras, G.E. Marnellos, Appl. Catal. B 138 (2013) 191–198.
[15] Y. Zhang, X. Wang, Y. Zhu, T. Zhang, Appl. Catal. B 129 (2013) 382–393.
[16] L.Z. Gao, C.T. Au, Appl. Catal. B 30 (2001) 35–47.
[17] K. Asano, C. Ohnishi, S. Iwamoto, Y. Shioya, M. Inoue, Appl. Catal. B 78 (2008) 242–249.
[18] E. Wilczkowska, K. Krawczyk, J. Petryk, J.W. Sobczak, Z. Kaszkur, Appl. Catal. A 389 (2010) 165–172.
[19] V.G. Komvokis, M. Marti, A. Delimitis, I.A. Vasalos, K.S. Triantafyllidis, Appl. Catal. B 103 (2011) 62–71.
[20] Y. Wu, X. Ni, A. Beaurain, C. Dujardin, P. Granger, Appl. Catal. B 125 (2012) 149–157.
[21] Y. Wu, C. Cordier, E. Berrier, N. Nuns, C. Dujardin, P. Granger, Appl. Catal. B 140 (2013) 151–163.
[22] M. Zabilskiy, P. Djinovic, B. Erjavec, G. Drazic, A. Pintar, Appl. Catal. B 163 (2015) 113–122.
[23] M. Iwamoto, H. Yahiro, Y. Mine, S. Kagawa, Chem. Lett. 18 (1989) 213–216.
[24] M. Iwamoto, H. Yahiro, Y. Torikai, T. Yoshioka, N. Mizuno, Chem. Lett. 19 (1990) 1967–1970.
[25] J. Perez-Ramirez, F. Kapteijn, G. Mul, J.A. Moulijn, Chem. Commun. 37 (2001) 693–694.
[26] G. Mul, M.W. Zandbergen, F. Kapteijn, J.A. Moulijn, J. Perez-Ramirez, Catal. Lett. 93 (2004) 113–120.
[27] P.J. Smeets, M.H. Groothaert, R.M. van Teeffelen, H. Leeman, E.J.M. Hensen, R.A. Schoonheydt, J. Catal. 245 (2007) 358–368.
[28] G.N. Li, E.A. Pidko, I.A.W. Filot, R.A. van Santen, C. Li, E.J.M. Hensen, J. Catal. 308 (2013) 386–397.
[29] M. Rutkowska, L. Chmielarz, M. Jablonska, C.J. Van Oers, P. Cool, J. Porous Mater. 21 (2014) 91–98.
[30] M. Rutkowska, L. Chmielarz, D. Macina, Z. Piwowarska, B. Dudek, A. Adamski, S. Witkowski, Z. Sojka, L. Obalova, C.J. Van Oers, P. Cool, Appl. Catal. B 146 (2014) 112–122.
[31] A. Ates, A. Reitzmann, G. Waters, Appl. Catal. B 119 (2012) 329–339.
[32] M.C. Campa, V. Indovina, D. Pietrogiacomi, Appl. Catal. B 111 (2012) 90–95.
[33] P. Boron, L. Chmielarz, J. Gurgul, K. Latka, T. Shishido, J.M. Krafft, S. Dzwigaj, Appl. Catal. B 138 (2013) 434–445.
[34] M. Iwamoto, H. Furukawa, Y. Mine, F. Uemura, S.I. Mikuriya, S. Kagawa, J. Chem. Soc. Chem. Commun. (1986) 1272–1273.
[35] Y. Kuroda, K. Yagi, N. Horiguchi, Y. Yoshikawa, R. Kumashiro, M. Nagao, Phys. Chem. Chem. Phys. 5 (2003) 3318–3327.

[36] A. Itadani, Y. Kuroda, M. Tanaka, M. Nagao, Micropor. Mesopor. Mater. 86 (2005) 159–165.
[37] P. Smeets, B. Sels, R. Vanteeffelen, H. Leeman, E. Hensen, R. Schoonheydt, J. Catal. 256 (2008) 183–191.
[38] E.M.C. Alayon, M. Nachtegaal, E. Kleymenov, J.A. van Bokhoven, Micropor. Mesopor. Mater. 166 (2013) 131–136.
[39] B.I. Palella, M. Cadoni, A. Frache, H.O. Pastore, R. Pirone, G. Russo, S. Coluccia, L. Marchese, J. Catal. 217 (2003) 100–106.
[40] M. Kogel, V.H. Sandoval, W. Schwieger, A. Tissler, T. Turek, Chem. Eng. Technol. 21 (1998) 655–658.
[41] X. Liu, Z.Y. Yang, R.D. Zhang, Q.S. Li, Y.P. Li, J. Phys. Chem. C 116 (2012) 20262–20268.
[42] S. Morpurgo, G. Moretti, M. Bossa, J. Mol. Catal. A 358 (2012) 134–144.
[43] M.L. Tsai, R.G. Hadt, P. Vanelderen, B.F. Sels, R.A. Schoonheydt, E.I. Solomon, J. Am. Chem. Soc. 136 (2014) 3522–3529.
[44] R.S. da Cruz, A.J.S. Mascarenhas, H.M.C. Andrade, Appl. Catal. B 18 (1998) 223–231.
[45] N. Liu, R.D. Zhang, B.H. Chen, Y.P. Li, Y.X. Li, J. Catal. 294 (2012) 99–112.
[46] X.Y. Zhang, Q. Shen, C. He, C.Y. Ma, J. Cheng, Z.M. Liu, Z.P. Hao, Catal. Sci. Technol. 2 (2012) 1249–1258.
[47] P.F. Xie, Z. Ma, H.B. Zhou, C.Y. Huang, Y.H. Yue, W. Shen, H.L. Xu, W.M. Hua, Z. Gao, Micropor. Mesopor. Mater. 191 (2014) 112–117.
[48] P.J. Smeets, Q. Meng, S. Corthals, H. Leeman, R.A. Schoonheydt, Appl. Catal. B 84 (2008) 505–513.
[49] H. Ohtsuka, T. Tabata, O. Okada, L.M.F. Sabatino, G. Bellussi, Catal. Lett. 44 (1997) 265–270.
[50] F. Seyedeyn-Azad, D.K. Zhang, Catal. Today 68 (2001) 161–171.
[51] D. Kaucký, J. Dědeček, B. Wichterlová, Micropor. Mesopor. Mater. 31 (1999) 75–87.
[52] J. Dědeček, D. Kaucký, B. Wichterlová, Micropor. Mesopor. Mater. 35 (2000) 483–494.
[53] J. Dědeček, L. Čapek, D. Kaucký, Z. Sobalík, B. Wichterlová, J. Catal. 211 (2002) 198–207.
[54] Z. Ma, Y. Ren, P.G. Bruce, J. Nanopart. Res. 14 (2012) 874 (11pp).
[55] L. Zhang, H.J. Liu, X.J. Li, S.J. Xie, Y.Z. Wang, W.J. Xin, S.L. Liu, L.Y. Xu, Fuel Process. Technol. 91 (2010) 449–455.
[56] X. Zhang, Q. Shen, C. He, Y.F. Wang, J. Cheng, Z.P. Hao, J. Hazard. Mater. 192 (2011) 1756–1765.
[57] X. Wang, H.Y. Chen, W.M.H. Sachtler, Appl. Catal. B 26 (2000) L227–L239.
[58] M. Mhamdi, S. Khaddar-Zine, A. Ghorbel, Appl. Catal. A 337 (2008) 39–47.
[59] N.V. Beznis, B.M. Weckhuysen, J.H. Bitter, Catal. Lett. 136 (2010) 52–56.
[60] W. Zou, P.F. Xie, W.M. Hua, Y.D. Wang, D.J. Kong, Y.H. Yue, Z. Ma, W.M. Yang, Z. Gao, J. Mol. Catal. A 394 (2014) 83–88.
[61] C. Chupin, A.C. van Veen, M. Konduru, J. Despres, C. Mirodatos, J. Catal. 241 (2006) 103–114.
[62] F. Bin, C.L. Song, G. Lv, J.O. Song, X.F. Cao, H.T. Pang, K.P. Wang, J. Phys. Chem. C 116 (2012) 26262–26274.
[63] T. Sun, M.L. Trudeau, J.Y. Ying, J. Phys. Chem. 100 (1996) 13662–13666.
[64] T.J. Chuang, C.R. Brundle, D.W. Rice, Surf. Sci. 59 (1976) 413–429.
[65] G. Fierro, M.A. Eberhardt, M. Houalla, D.M. Hercules, W.K. Hall, J. Phys. Chem. 100 (1996) 8468–8477.
[66] L. Guczi, D. Bazin, Appl. Catal. A 188 (1999) 163–174.
[67] Z. Zsoldos, L. Guczi, J. Phys. Chem. 96 (1992) 9393–9400.
[68] N. Pasha, N. Lingaiah, P.S.S. Reddy, P.S.S. Prasad, Catal. Lett. 127 (2009) 101–106.
[69] H.B. Zhou, Z. Huang, C. Sun, F. Qin, D.S. Xiong, W. Shen, H.L. Xu, Appl. Catal. B 125 (2012) 492–498.
[70] J. Dědeček, B. Wichterlová, J. Phys. Chem. B 103 (1999) 1462–1476.
[71] L. Drozdová, R. Prins, J. Dědeček, Z. Sobalík, B. Wichterlová, J. Phys. Chem. B 106 (2002) 2240–2248.
[72] L.F. Cordoba, G.A. Fuentes, C.M. de Correa, Micropor. Mesopor. Mater. 77 (2005) 193–201.
[73] V. Indovina, M.C. Campa, D. Pietrogiacomi, J. Phys. Chem. C 112 (2008) 5093–5101.
[74] A.A. Verberckmoes, B.M. Weckhuysen, R.A. Schoonheydt, Micropor. Mesopor. Mater. 22 (1998) 165–178.
[75] J. Vakros, C. Kordulis, A. Lycourghiotis, Langmuir 18 (2002) 417–422.
[76] L.F. Liotta, G. Pantaleo, A. Macaluso, G. Di Carlo, G. Deganello, Appl. Catal. A 245 (2003) 167–177.
[77] X.Y. Zhang, Q. Shen, C. He, C.Y. Ma, J. Cheng, Z.P. Hao, Catal. Sci. Technol. 2 (2012) 1059–1067.
[78] A.V. Boix, S.G. Aspromonte, E.E. Miro, Appl. Catal. A 341 (2008) 26–34.
[79] F. Kapteijn, G. Marban, J. RodriguezMirasol, J.A. Moulijn, J. Catal. 167 (1997) 256–265.
[80] J.B. Nagy, Z. Gabelica, G. Debras, E.G. Derouane, J.P. Gilson, P.A. Jacobs, Zeolites 4 (1984) 133–139.
[81] F. Deng, Y.R. Du, C.H. Ye, J.Z. Wang, T.T. Ding, H.X. Li, J. Phys. Chem. 99 (1995) 15208–15214.
[82] S. Altwasser, J. Jiao, S. Steuernagel, J. Weitkamp, M. Hunger, Stud. Surf. Sci. Catal. 154 (2004) 3098–3105.
[83] J. Caro, M. Noack, J. Richtermendau, F. Marlow, D. Petersohn, M. Griepentrog, J. Kornatowski, J. Phys. Chem. 97 (1993) 13685–13690.
[84] G. Muller, T. Narbeshuber, G. Mirth, J.A. Lercher, J. Phys. Chem. 98 (1994) 7436–7439.